Energy Resolution of Scintillators in Connection With Track Structure

Aleksandr Gektin, *Member, IEEE*, Andrey N. Vasil'ev, Victor Suzdal, and Aleksandr Sobolev

***Abstract*— The large spread of scintillator performance (light yield and energy resolution) from a theoretical limit shows that we are still far from the deep understanding of the phenomena. Usually, extrinsic aspects of resolution degradation (such as purity, defects, stoichiometry, and so on) are the subject of study. At the same time, intrinsic factors (such as track structure, excitation density, and uniformity) that depend on crystal lattice can play a dominant role in scintillator performance. Some progress in the understanding of these problems is achieved by using the concept of different efficiencies of photon emission from excited regions with different concentrations of electronic excitations. The regions with a high or low concentration of thermalized excitations result in the nonradiative losses of excitations and, therefore, produce additional event-to-event fluctuations. The technique of multidimensional analysis of the time-resolved pulse shape is proposed for the clustering of all the events according to the proximity of the waveform to some centroids of the clusters. This procedure shows that even conventional NaI:Tl and CsI:Tl scintillators allow to achieve an energy resolution of about 3% for 662-keV gamma photons.**

***Index Terms*— Decay kinetics, electronic excitations, energy resolution, scintillators.**

I. Introduction

ENERGY resolution of scintillation detectors is a crucial parameter for spectrometry devices for multiple isotope distinguishing [1]–[3]. Energy resolution is also an important characteristic of scintillation detectors in various applications. Fig. 1 shows a significant spread of light yield and energy resolution values of NaI:Tl industrial detectors. More and more attempts [4]–[5] are directed toward resolution improvement by crystal purification, codoping, and other technological methods [5]–[7]. The best results at about 5.0%–5.5% (^{137}Cs source) [4]–[5] are still very far from the fundamental limit (about 2.6% [8]). Nevertheless, low-temperature tests [9] demonstrate an ability to reach a better experimental value of resolution (∼4%) and a light yield of two times higher than at room temperature. The physical reasons for the increase in resolution are not clear and the possibility to significantly improve this parameter is still questionable.

Manuscript received January 25, 2020; revised February 28, 2020; accepted February 28, 2020. Date of publication March 4, 2020; date of current version June 19, 2020.

Aleksandr Gektin, Victor Suzdal, and Aleksandr Sobolev are with the Institute for Scintillation Materials, 61001 Kharkov, Ukraine (e-mail: gektin@yahoo.com).

Andrey N. Vasil'ev is with the Skobeltsyn Institute of Nuclear Physics, Lomonosov Moscow State University, 119991 Moscow, Russia (e-mail: anv@sinp.msu.ru).

Color versions of one or more of the figures in this article are available online at http://ieeexplore.ieee.org.

Digital Object Identifier 10.1109/TNS.2020.2978236

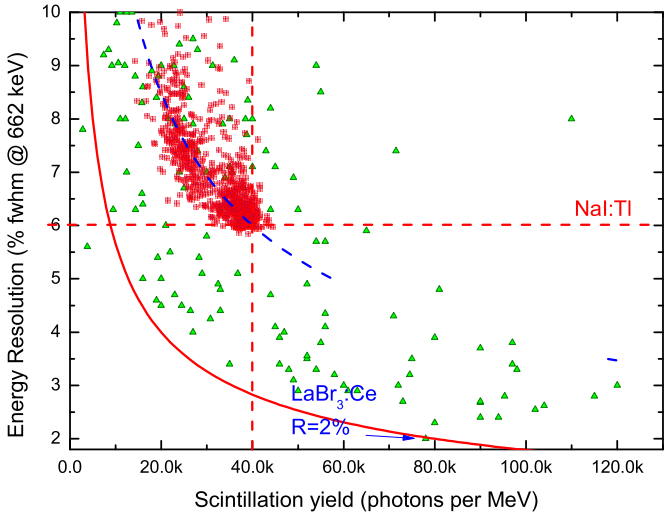

Fig. 1. Spread of energy resolution data and light yield for 800 samples of NaI:Tl grown at the same technology (circles) together from the corresponding data for different scintillators from [3]. Red line shows the theoretical limit for energy resolution.

The origin of the energy resolution was discussed in the early 1960s [10], [11]. Starting from the end of the 1990s, the connection of energy resolution with material properties was intensively studied [8], [12]. One of the main ideas was that the energy resolution is totally defined by the scintillation yield nonproportionality. Indeed, gamma rays produce a set of electrons of different energies when they interact with a detector. Fluctuations of specific electron energies in the set between different events should broaden the energy resolution in case of electron yield nonproportionality [12]. There is an evident correlation between nonproportionality and energy resolution (see, e.g., [13] where data from a systematic study of low-energy yield nonproportionality [14] were used). During the following years, electron yield nonproportionality was investigated for many crystals both experimentally and theoretically [14]–[29]. These studies provide an explanation of how nonproportionality is connected with material parameters (for instance, thermalization length of hot electrons) and how yield and decay kinetics are modified with the energy of the primary ionizing particle. These investigations used the rate equations in cylindrical form of the track accounting for the separation of charged carriers, some kinds of Monte Carlo estimations, and underlined the role of local concentrations of carriers created after thermalization. Unfortunately, these studies did not provide guidelines on how to improve the energy resolution of existing commercial scintillators.

All attempts to alter the materials or modify technology to improve energy resolution, while keeping the cost low, did not bring us closer to the fundamental limit. Another possible way to achieve this goal is to try to use pulse shape information to improve energy resolution value [30]–[33]. This idea is based on the dependence of decay kinetics on the energy of created electrons and on the topology of the tracks generated in different events (see [30, Fig. 7] and [33, Figs. 2 and 5]).

The pulse shape discrimination is known from the end of the 1960s [34], and is used for some cases [35], but still needs deeper understanding and development. This information can improve resolution data, but again, we are still very far from the limit.

Nevertheless, the idea that energy resolution is totally determined by nonproportionality seems to be oversimplified since the approach developed in [12] supposes that the yield from different secondary electrons is just summarized. If the excited regions of several electrons overlap, the resulting scintillation yield will not be presented by the sum of individual yields of each of the electrons. Most of the theoretical approaches previously mentioned do not take into account the event-to-event fluctuations of the overall excited regions.

During the past years, the series of works are devoted to deeper investigation of nonuniformity distribution of excitations and their later relaxation depending on different irradiation conditions [31], [32]. It was shown that the nonuniformity of electron densities in the particle tracks is very sensitive to all the stages of electron relaxation. The average distance between the excitations in different parts of the track can differ from several angstroms to hundreds of nanometers corresponding to the effective excitation density from 10^{22} to 10^{13} excitations per cubic centimeter. In addition, this track structure changes from event to event [36]. The analysis presented in [36] shows that how different spatial regions with different excitation densities influence both yield and energy resolution. For a high density of excitations, the quenching increases and the decay kinetics is shorter than the characteristic radiative time of the emitting center. At the same time, the dispersion of the number of photons emitted from these regions also increases. The low-density regions result in an increase of slow components of the scintillation decay. A part of the photons is emitted beyond the detection time, resulting in an increased noise. In other words, significant variations of the density distribution of excitations in the track region from one event to another could be the reason for energy resolution deterioration. We believe that nonmonotonic and nonproportionality curves in alkali halide crystals and rather poor energy resolution of these crystals have the same origin [36], namely the distribution of local concentrations of excitations and their event-to-event fluctuations.

The simplest way to take advantage of the pulse shape analysis to improve the energy resolution is the weighting of signals obtained in some time domains (e.g., fast, intermediate, and slow, as proposed in [30] and [36]). Nevertheless, the problem of choosing weight coefficients and length of time domains has no simple solution since theoretical models can give only the illustrative estimations. Even detailed multiparameter models (e.g., [30]) should be tuned for each specific scintillator. At present, each scintillation pulse can be digitized with high precision (e.g., [37], [38]), and it is promising to take advantage of such possibility. The powerful statistical techniques of treating big data can be useful in the analysis of this information.

In the frame of this article, we tried to resolve two problems. First of all, we show that even simple models of the formation of decay curves on the simulated track structure can provide illustrative information about the connection of track structure with decay curves, which is not straightforward. In Section II, we present an event-to-event change of the simulated decay curves in NaI:Tl. The main result of this section is the demonstration of a certain correlation between the amplitude and decay curve for each event. In Sections III and IV, we develop a "data mining" approach to the treatment of individual decay data and decay vector, which represents each decay (preliminary results were presented in [39]). The approach consists of the clustering of decay vectors without preliminary knowledge of the model of scintillation. Each new event can be attributed to one of the clusters, and in this way, the energy resolution can be significantly improved. The experiment was performed on the data obtained for NaI:Tl and CsI:Tl. In the conclusion, we emphasize on the potential and restrictions of the proposed technique.

II. Influence of the Track Structure on the Photopeak Broadening

In order to simulate tracks and decay kinetics, we use the technique [31], [32], [36], which differs from the model of cylindrical track with smooth distribution of excitations along the track, used in [15], [16], and [19]. The selected approach has some limitations since it does not take into account the electric fields originating from the separation of electrons from holes, but it takes into account the microscopic structure of the track, such as clustering of carriers, due to Auger cascade and production of δ-electrons, and allows simulating noncylindrical tracks.

The fluctuation of track structure from event to event and the corresponding fluctuation of the scintillator yield and decay kinetics were studied based on the Monte Carlo simulation of the track structure. The calculations were performed for 66 events of 200-keV electron tracks in NaI. Coordinates of electrons and holes after their thermalization were calculated as described in detail in [31], [32], and [36]. First of all, the energy loss functions for NaI were simulated based on EPDL97 database [40] of photoelectron cross sections with corrections of energies of NaI core and valence states in order to reproduce forbidden gap and core band energies in NaI. Monte Carlo simulation of the cascade of electron–electron scattering with the production of secondary electrons and holes from the valence band and core bands was performed with taking into account the momentum conservation in each collision. These calculations result in spatial coordinates of electrons and holes together with their kinetic energies after the "last" inelastic scattering, i.e., when their kinetic energy is not sufficient to produce additional electronic excitation. This means that cascade stage of simulation is finished when

the kinetic energy of the particle becomes lower than the forbidden gap energy, which is the threshold for inelastic electron–electron scattering. The next stage is the account for thermalization with the emission of phonons. At this stage, the position of an electron or a hole is shifted in an arbitrary direction. Its "final" position is determined in correspondence with thermalization length, which depends on the kinetic energy of the particle [41]. For most scintillators, holes are heavier than electrons, and their kinetic energy is limited by the width of the valence band, so their thermalization length is typically much less than that for electrons.

The next step for the estimation of the scintillation yield and decay kinetics is the calculation of the distribution of efficient concentrations in the track region. The aim of this calculation is to determine how far electrons should diffuse toward holes and then recombine. An efficient concentration can be defined from the mean distance between an electron and the nearest one, two, three, or more holes. In the present estimation, we calculate the mean distance $\langle r_{eh}\rangle_3$ to three nearest holes for each electron. The "concentration" which an electron feels in this case is $(\langle r_{eh}\rangle_3)^{-3}$. The distribution of concentrations is calculated in such a way and is presented for all 66 tracks in the left panel of Fig. 2 showing the histogram over equidistant $\ln(n)$ bins. Therefore, the area under blue curves corresponds to the total number of initial electron–hole pairs.

For the estimation of yield and decay kinetics, we use the simplest analytical model, which describes the electron–hole recombination and exciton–exciton quenching [42]. The case of NaI:Tl scintillator is definitely more complicated, and the corresponding rate equations are studied in [17] and [43]–[45]. Nevertheless, we use here the simplified model since the number of parameters for this model is much lower and it is easier to get qualitative results depending on the small set of important parameters. The parameters of this model are the exciton radiation time $\tau_{\rm rad}$, binominal rate of electron–hole recombination g_{eh}, binominal rate of exciton–exciton quenching $b_{\rm ex}$, and time of integration of the scintillation response $t_{\max}$. The set of equations for electron and hole concentrations ($n_e(t) = n_h(t)$) is

$$\frac{dn_{\rm ex}(t)}{dt} = -\frac{1}{\tau_{\rm rad}} n_{\rm ex}(t) - b_{\rm ex} n_{\rm ex}^2(t) + g_{eh} n_e(t) n_h(t)$$
$$\frac{dn_e(t)}{dt} = -g_{eh} n_e(t) n_h(t).$$

For estimations, we choose $\tau_{\rm rad} = 1$ μs, $b_{\rm ex} = 10^{-19}$ s^{-1} cm^{-3}, $g_{eh} = 10^{-16}$ s^{-1} cm^{-3}, and $t_{\max} = 5$ μs. We suppose that excitons are not produced in the cascade ($n_{\rm ex}(0) = 0$). The analytical solution of this set of equations is rather cumbersome and is presented in [42]. The efficiency of emission and registration of photon $q(n)$ from region with initial concentration of electrons $n_e(0)$ is calculated using the previously mentioned rate equations and, for chosen parameters, is shown by a red line in the left panel of Fig. 2, whereas the average decay kinetics of the scintillation is shown in the right panel of Fig. 2. This kinetics is obtained as the integral of partial decays for different $n_e(0)$ over the distribution of concentrations averaged for all

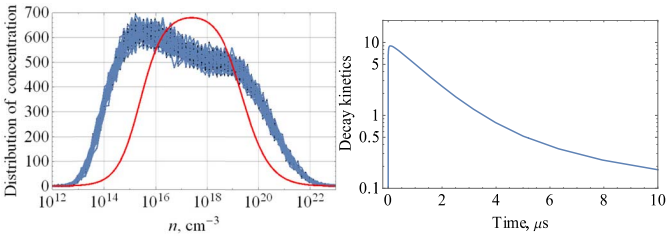

Fig. 2. Left: distribution of electron concentration in the track regions for 66 tracks of 200-keV electrons in NaI (blue curves) and the efficiency of emission and detection of photons originating from the regions with different electron concentrations (red curve, multiplied by 700 for the visibility on the plot). Right: averaged scintillator decay kinetics for model with electron-hole recombination and exciton-exciton quenching (parameters presented in the text). Calculation is based on the distribution of electron concentrations presented in the left panel.

simulated tracks. The parameters are chosen in a way to roughly reproduce typical NaI:Tl decay kinetics (compare the right panel of Fig. 2 with Figs. 4 and 6 presented in Section IV below). The efficiency of emission and registration of photons reaches its maximum close to 1 at an initial concentration about 10^{17} cm^{-3}. For higher concentrations, the efficiency of photon emission by excitons drops due to the exciton–exciton quenching. For lower concentrations, the electron–hole recombination becomes too slow, and the photons are emitted at times much higher than the pulse integration time. The decay has different components. For concentrations about 10^{17} cm^{-3}, the decay is about monoexponential with small rising time. For lower concentrations, the decay has a longer rising part and a long tail. Finally, for higher concentrations, the decay has a fast rising part and an accelerated initial part. The integration over distribution of concentrations in the track region results in a complex shape of the decay.

The simulated tracks differ in the number of electron–hole pairs and their spatial structures. Therefore, the distribution of concentrations fluctuates from one track to another, and the yield and decay also fluctuate. The mean number of electron–hole pairs $\langle N_{eh}\rangle$ for the simulations of 200-keV electron tracks is 24304 (121×10^3 e–h pairs per MeV), with the standard deviation σ_{eh} equal to 35. The Fano factor $F_{eh} = \sigma_{eh}^2/\langle N_{eh}\rangle = 0.053$. This result corresponds to the figures obtained in [46]. Mean scintillator yield for the chosen parameters of rate equations is $\langle Y\rangle = 14022$ (70×10^3 photons per MeV), with standard deviation σ_Y equal to 97, and the corresponding Fano factor $F_Y = \sigma_Y^2/\langle Y\rangle = 0.67$. The fluctuations of the yield are much higher than the fluctuations of the number of carriers. This is due to the fluctuations of the track structure. This result does not include the noise due to photon generation and registration in different regions of the track, which is proportional to $\sqrt{q(n)(1-q(n))}$ and which can be significant (see [36]).

The calculated scintillation yields for different tracks are shown in the top right panel of Fig. 3. In order to find out whether there are correlations between yield, track structure, and decay kinetics, we divide the tracks into three groups, which give different yield: $Y > \langle Y\rangle + 0.8\sigma_Y$ (green points,

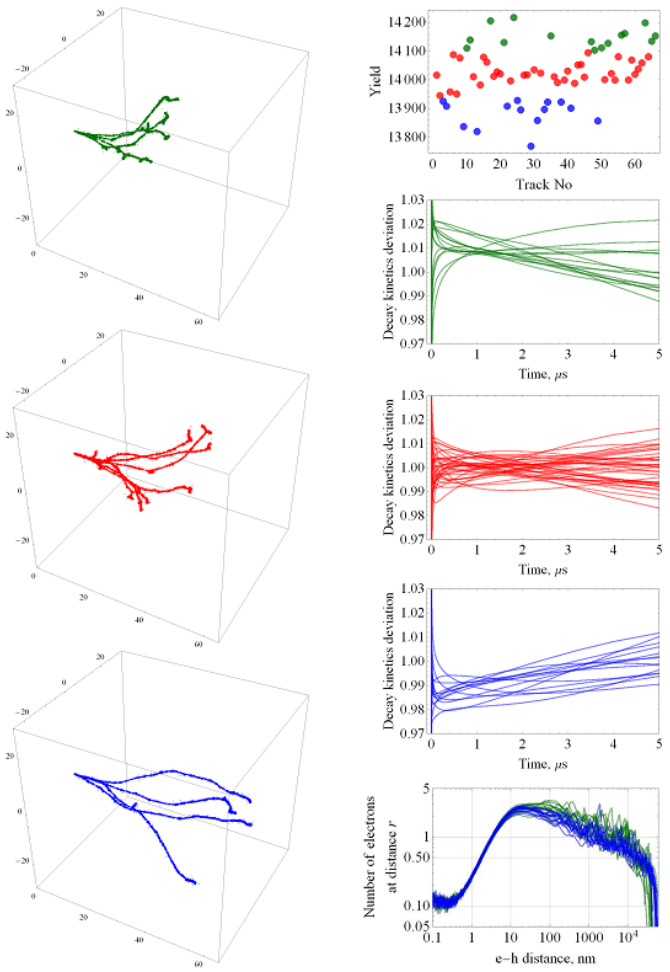

Fig. 3. Illustration of the relation between track structure, simulated scintillation yield and deviation of decay kinetics for 66 tracks of 200-keV electrons in NaI. Left: typical spatial distribution of electrons. From top to bottom: four examples of tracks resulting in yield $Y > \langle Y\rangle + 0.8\sigma_Y$ (green points in the right top panel), six tracks with $\langle Y\rangle - 0.8\sigma_Y < Y < \langle Y\rangle + 0.8\sigma_Y$ (red points), and four tracks with $Y < \langle Y\rangle - 0.8\sigma_Y$ (blue points). Right: Simulated yield Y for different tracks (top panel), grouped by color in three previously mentioned regions. Three middle panels: the ratio of simulated kinetics to mean kinetics for three previously mentioned groups of the yield. Bottom panel: distribution of number of electrons per 1 nm of electron-hole distance for different tracks from the group with $Y > \langle Y\rangle + 0.8\sigma_Y$ (green curves) and $Y < \langle Y\rangle - 0.8\sigma_Y$ (blue curves).

right part of scintillation photopeak), $\langle Y\rangle - 0.8\sigma_Y < Y < \langle Y\rangle + 0.8\sigma_Y$ (red points, middle part of photopeak), and $Y < \langle Y\rangle - 0.8\sigma_Y$ (blue points, left part of photopeak). The boundaries $0.8\sigma_Y$ are chosen because for Gaussian distribution of the yields, about 40% of events have yields outside the central interval. In order to obtain a correlation of the yield with track structure and decay features, we plot tracks and decay curves in the same colors. Typical tracks which correspond to these three groups are presented in the left column. The tracks with higher yield are shorter and show more dense regions with a larger number of clusters of excitations (“spurs”) (green, left top panel). On the contrary, tracks with lower yield are characterized by larger length and more straight structure (left bottom panel, blue). These tracks are characterized by a different spatial dependence of the number of electrons per one nanometer of electron–hole distance (bottom right panel). Such a different spatial structure is also reflected in decay kinetics. Three middle figures in the right column show the ratio of the calculated decay kinetics to average decay kinetics as shown in the right panel of Fig. 2. The tracks with high yield (green points and curves) are characterized by the reduction of long components (at $\sim$5 μs) in comparison with middle components ($\sim$1 μs) of the decay. On the contrary, the tracks with low yield (blue points and curves) show some increase of long components in comparison with medium-time components.

Definitely, we cannot practically improve the energy resolution by selecting events with specific track structure since it is not observable directly. Nevertheless, one of the observable characteristics of the emission from the track region is the shape of the scintillation pulse. We can measure only decay kinetics and in this way attribute each event to one of three groups. Fig. 2 shows that the decay kinetics is not connected in one-to-one way with the value of the yield, and it is just a statistical correlation. It reflects the complex structure of photopeak. The different events of the interaction of gamma photon with the crystal result in additional broadening of the peak beyond the statistics of electron–hole pairs. Therefore, the main question is whether a statistical approach to scintillation events analysis can separate different topologies of the tracks.

III. Technique for the Treating of Pulse Amplitude Spectra

The standard method for measuring the result of the interaction of an ionizing particle with a scintillator is to construct the amplitude spectrum of scintillation pulses. With this approach, the signal from each event (scintillation resulting from an ionizing particle or a gamma quantum interaction with media) at the output of the photodetector is integrated in a given interval of time, and each event corresponds to one value–pulse amplitude. Using the obtained array of scalar values, a histogram of the distribution is constructed, which is the amplitude spectrum. Section II demonstrates that the kinetics of the scintillation pulse is affected by the structure of the track of an ionizing particle. If we group individual decays according to their proximity to some “calibrated” profiles, corresponding to groups with high, medium, and low amplitudes of the scintillation pulse, we can hope to increase the energy resolution for each group of events.

The kinetics of each scintillation pulse can be digitized using contemporary digital oscilloscopes. Therefore, each event can be characterized by the vector of the digitized values. These vectors can then be treated using a modern algorithm of data processing [47]–[49]. These algorithms allow clustering of the events without any *a priori* knowledge of the models. Therefore, the procedure consists of two steps: the first step is the “learning” procedure, when a big amount of events are treated in order to form some clusters of events, and then we can treat each new event according to its proximity to the centroids of each cluster.

Clustering procedure is widely used in the systems of artificial intelligence and data mining problems [48], [49]. The term “data mining” appeared around the 1990s in the

database community and became more popular in the artificial intelligence and machine learning community. The clustering of data and the following analysis of them are successfully used in the problems of visualization of hidden dependences, structuration of data, distinguishing acting factors without their analytical description, and so on. Clustering procedure implies decomposition (dissection) of the data array in the parameter area. Section planes are set by the selected norms, by which the distances between primitives (data array elements) are calculated. Implementations of the clustering procedure can be very diverse and have a significantly different computational complexity, different convergence, and accuracy of solutions. Currently, data mining methods are well developed, have a large number of applied tools (method implementations) [50]–[52], integrated into mathematical packages, such as MATLAB, Scilab, and others. Extensive Python software libraries (SciPy and NumPy) [53], and C and many other languages which implement data mining methods, including the clustering methods used by the authors, are available. The authors do not describe the methods and algorithms of clustering because they did not develop them but directly applied them to the field of processing data from scintillation experiments.

IV. Experiment and Results

In the frame of this study, both conventional scintillation spectra method and a new one, based on discretization of the pulse shape of individual events, were used for different scintillators. In particular, three most popular scintillators were selected for the series of comparative tests —NaI:Tl, CsI:Tl, and CsI:Na. Three groups of each type of crystals (selected quality—resolution for ^{137}Cs source of 5.5%–6.0%, standard quality—6.5%–7.0%, and low quality—worse than 7.5%–8.0%) were selected for the tests. Cylindrical samples Ø1" × 1" were prepared for spectra measurement at room temperature. Spectral measurements were performed using a standard analog approach at multichannel analyzer, model Multiport II (Canberra) with standard Hamamatsu photomultiplier (PMT) HM R1308 2" (HV: 1075 V) or with fast PMT ET 9821B 3" (HV: 2085 V). Digital oscilloscope, LeCroy waveSurfer 422, 200 MHz, 2 gigasample/s type, was used for recording individual events. A total of 99 000 events were used for each test. All together, more than 100 tests were performed. In these experiments, digitized scintillation pulses were used without preliminary filtering by area or amplitude. The maximum recording speed was 33–35 pps. The input impedance of the oscilloscope in all measurements was 50 Ω.

The typical approach is based on the following procedure. The digitized pulse with digitizing frequency 0.3 gigasample/s was integrated over 100-ns integrals (Fig. 4). Thus, each scintillation event was associated with a vector containing partial sums of the signal value. Therefore, instead of a single number characterizing the scintillation amplitude (the integral of the signal during shaping time), the event is characterized by a vector of a sufficiently large dimension (in our case, 24). We assume that an even smaller number of integration intervals will give satisfactory statistics. The aggregate of all

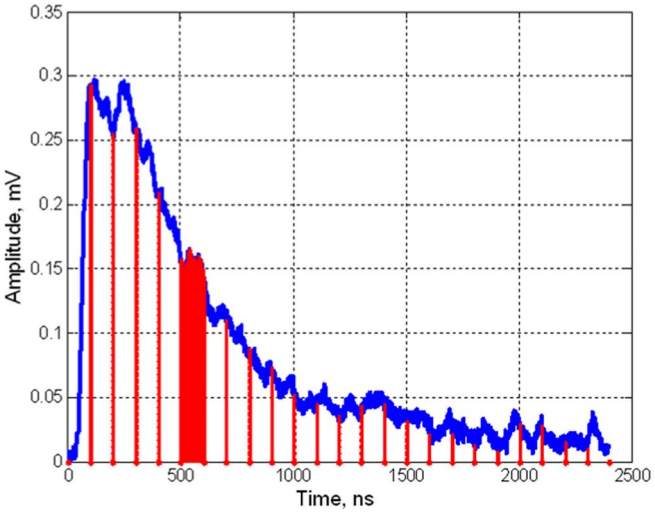

Fig. 4. Example of digitized NaI:Tl scintillation pulse and a scheme of the formation of the data vector for the event.

scintillation events can be described by a set of corresponding vectors, in the first case in a 1-D event space and in the second in a multidimensional one.

The idea of further data treatment is quite simple. Events are subdivided into several groups depending on specific decay time, decay character, character and speed of the rising leading edge and maximum amplitude, and so on.

In our case, we chose the simply constructed multidimensional vector corresponding to the digitization of the scintillation signal. A mathematical measure of proximity is a norm, the choice of which allows to control the criterion for the formation of groups (Euclidean, soft cosine, correlation, and many other norms can be used). We use squared distance and Euclidean distance as metrics for two vector describing events. As indicated earlier, the described procedure is collectively called "clustering," and the resulting groups are clusters. Naturally, these clusters of events have nothing to do with the spatial clusters of electronic excitations mentioned in the description of the track structure. As a result of such clustering, events that are characterized by close decay kinetics are grouped in the same cluster.

If we construct the distribution of the amplitudes of the scintillation signal for each of the events in the cluster and compare this distribution with the distribution of the amplitudes for all events (Fig. 5), then we can see that the events in the clusters constructed by the proximity of the shape of the decay curves of the scintillation signal are also characterized by different distributions of the amplitude of the scintillation signal. The amplitude distributions for different clusters are partially overlapped. This fact correlates with the comment made in Section II that some tracks shown in green and blue demonstrate the "wrong" decay behavior (there is no one-to-one correspondence between decay and the yield). Fig. 6 shows the average kinetics for each of the clusters (cluster centroids in the language of the data processing technology). It can be seen that the clusters are characterized by a different signal ratio at time domains 500–1000 ns to

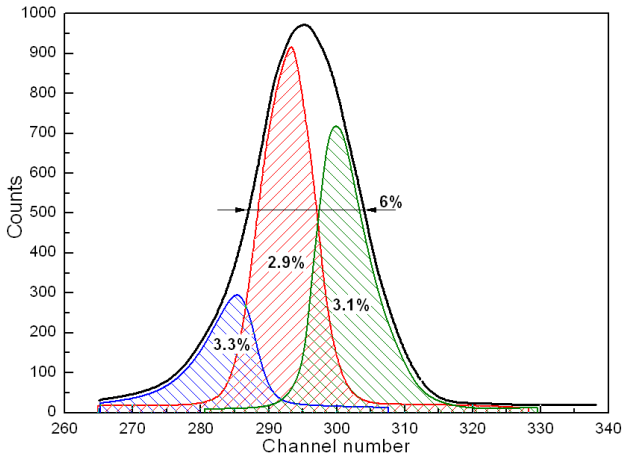

Fig. 5. Example of decomposition of the ^{137}Cs full absorption peak in amplitude spectrum by three clusters.

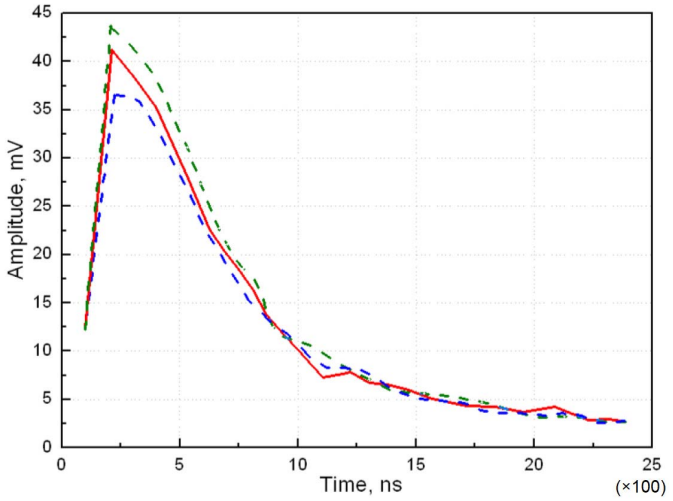

Fig. 6. Reconstruction of centroids of pulse clusters.

2000–2500 ns. Thus, selecting only one cluster from the total number of events and taking the amplitudes of events in this cluster, one can significantly improve the energy resolution. In addition, it is possible to take into account all the events preserving improved resolution by introducing correction for the contributions of all the clusters.

Different curves for centroids at each peak correlate with the trends of the decay curves described in Section II and with the role of fast and slow components of decay shown in [30]. In particular, a cluster with lower amplitude (blue curves) is characterized by a low value of intermediate-to-fast ratio, which corresponds to the result shown in Fig. 3 (fourth panel in the right column). The same correlation between simulation and experiment is obtained for a cluster with high amplitudes.

Table I shows the results of event processing for different materials and energy resolutions of crystals. The first row presents the energy resolution without mathematical processing of the kinetics. The second one shows the results of clustering–selection of events characterized by proximity to the centroid of the central cluster.

TABLE I
RESULTS OF THE TREATMENT OF SCINTILLATION EVENTS

Material	NaI:Tl	NaI:Tl	CsI:Tl	CsI:Tl
Raw resolution, %	5.82	5.54	7.40	10.44
Resolution after treatment, %	3.01	2.83	3.88	5.35

The values of the energy resolution of the peaks constructed from clusters are better than those for the amplitude peaks constructed from the entire set of scintillation pulses. The central cluster peak is usually the largest in area and has an energy resolution close to a theoretically predicted one. Our experiments show that the subdivision into three clusters is sufficient to reproduce the structure of a photopeak, and the clustering components have half-widths close to the theoretical limit for a given substance.

There are no direct criteria for the selection of the number of clusters. Experiments show that photopeak parameters in the case of NaI and CsI scintillators improve up to three clusters' selection and remain constant for larger (up to nine clusters) number of clusters.

V. CONCLUSION

The energy resolution of scintillating crystals is affected both by intrinsic and extrinsic factors. By intrinsic factors, we mean event-to-event fluctuations of the spatial distribution of excitations. This distribution is known to define both the yield nonproportionality and nonexponential profile of decay kinetics, especially components much shorter and much longer than characteristic decay time of emission centers [16], [30], [36], and in this article, we show that event-to-event fluctuations play an important role in the deterioration of the energy resolution. The correlation of the decay kinetics with the yield demonstrated using Monte Carlo simulation of the track structure can be used to correct the yield of individual events to improve the energy resolution. At the same time, the practice shows that the energy resolution measured for different crystals grown using the same technology differs significantly [54] due to extrinsic factors. Therefore, here we propose a technique of treating the scintillation signals which is based on the previously mentioned correlation between signal waveform and the total scintillation yield but which also takes into account uncontrolled reasons of the deterioration of energy resolution.

It is shown that, in contrast to analog scintillation spectrum processing methods, digital methods provide enhanced possibilities. Naturally, the accumulation of a large amount of digital data requires big digital arrays but, at the same time, makes it possible to radically improve scintillation detector performance. The proposed method for the analysis and construction of the scintillation spectrum makes it possible to reveal a nonelementary structure of photopeaks. In other words, the statistical approach shows that not all events, even within one peak, are equivalent. This follows already from modeling the nonuniformity of the track itself, and of course, is reflected in the intricacies of the photopeak structure.

In particular, it was shown that the most popular alkaline halide scintillators have a complex character of scintillation generation, and the integration of all manifestations together leads to the broadening (smearing) of the photopeak. It is important to note that the separation of processes due to the clustering of statistical information leads to the identification of energy resolution parameters close to the theoretical limit.

Analysis of the spectra integrated at different stages of the decay kinetics of the scintillation pulse shows that it is possible to separate different processes forming the photopeak, thus improving energy resolution. The Monte Carlo simulation shows the correlation of the yield and the decay profile, and a similar correlation is obtained by numerical treatment of experimental data. The results of Section II demonstrate that numerical clustering presented in Sections III and IV is physically meaningful.

Although all experiments were performed for alkali halide scintillators, there are no limits to apply this approach to other types of scintillators. This procedure is appropriate for scintillators with energy resolution far from theoretical limit.

REFERENCES

[1] G. F. Knoll, *Radiation Detection and Measurement*, 3rd ed. New York, NY, USA: Wiley, 2000.

[2] P. Lecoq, A. Gektin, and M. Korzhik, "Inorganic scintillators for detector systems," in *Physical Principles and Crystal Engineering*. Cham, Switzerland: Springer, 2017, p. 408.

[3] S. Derenzo, M. Boswell, M. Weber, K. Brennan, *Scintillation Properties Database*. Accessed: Jan. 20, 2020. [Online]. Available: http://scintillator.lbl.gov

[4] K. Yang and P. R. Menge, "Improving γ-ray energy resolution, non-proportionality, and decay time of NaI:Tl^{+} with Sr^{2+} and Ca^{2+} co-doping," *J. Appl. Phys.*, vol. 118, no. 21, 2015, Art. no. 213106.

[5] I. V. Khodyuk, S. A. Messina, T. J. Hayden, E. D. Bourret, and G. A. Bizarri, "Optimization of scintillation performance via a combinatorial multi-element co-doping strategy: Application to NaI:Tl," *J. Appl. Phys.*, vol. 118, no. 8, Aug. 2015, Art. no. 084901.

[6] M. Nikl and A. Yoshikawa, "Recent R&D trends in inorganic single-crystal scintillator materials for radiation detection," *Adv. Opt. Mater.*, vol. 3, no. 4, pp. 463–481, 2015.

[7] T. Shalapska, F. Moretti, E. Bourret, and G. Bizarri, "Effect of Au codoping on the scintillation properties of BaBrCl:Eu single crystals," *J. Lumin.*, vol. 202, pp. 497–501, Oct. 2018.

[8] P. Dorenbos, J. T. M. de Haas, and C. W. E. van Eijk, "Non-proportionality in the scintillation response and the energy resolution obtainable with scintillation crystals," *IEEE Trans. Nucl. Sci.*, vol. 42, no. 6, pp. 2190–2202, Dec. 1995.

[9] P. Sibczynski, M. Moszynski, T. Szczesniak, W. Czarnacki, A. Syntfeld-Kazuch, and P. Schotanus, "Further study of undoped NaI scintillators with different purity," in *Proc. IEEE Nucl. Sci. Symp. Med. Imag. Conf.*, Oct. 2010, pp. 574–579.

[10] C. D. Zerby, A. Meyer, and R. B. Murray, "Intrinsic line broadening in NaI(Tl) gamma-ray spectrometers," *Nucl. Instrum. Methods*, vol. 12, pp. 115–123, Jun./Jul. 1961.

[11] J. R. Prescott and G. H. Narayan, "Electron responses and intrinsic linewidths in NaI(Tl)," *Nucl. Instrum. Methods*, vol. 75, no. 1, pp. 51–55, Nov. 1969.

[12] B. D. Rooney and J. D. Valentine, "Scintillator light yield nonproportionality: Calculating photon response using measured electron response," *IEEE Trans. Nucl. Sci.*, vol. 44, no. 3, pp. 509–516, Jun. 1997.

[13] M. Moszyński *et al.*, "Energy resolution of scintillation detectors," *Nucl. Instrum. Methods Phys. Res. A, Accel., Spectrometers, Detectors Associated Equip.*, vol. 805, pp. 25–35, Jan. 2016.

[14] I. V. Khodyuk and P. Dorenbos, "Trends and patterns of scintillator nonproportionality," *IEEE Trans. Nucl. Sci.*, vol. 59, no. 6, pp. 3320–3331, Dec. 2012.

[15] X. Lu *et al.*, "Coupled rate and transport equations modeling proportionality of light yield in high-energy electron tracks: CsI at 295 K and 100 K; CsI:Tl at 295 K," *Phys. Rev. B, Condens. Matter*, vol. 92, no. 11, Sep. 2015, Art. no. 115207.

[16] X. Lu *et al.*, "Energy-dependent scintillation pulse shape and proportionality of decay components for CsI:Tl: Modeling with transport and rate equations," *Phys. Rev. Appl.*, vol. 7, no. 1, Jan. 2017, Art. no. 014007.

[17] S. Kerisit, Z. Wang, R. T. Williams, J. Q. Grim, and F. Gao, "Kinetic Monte Carlo simulations of scintillation processes in NaI(Tl)," *IEEE Trans. Nucl. Sci.*, vol. 61, no. 2, pp. 860–869, Apr. 2014.

[18] J. Singh, R. T. Williams, A. Koblov, and D. Surovtseva, "Effect of time-dependent local excitonic concentration in the track on nonproportionality in light yield of inorganic scintillators," *IEEE Trans. Nucl. Sci.*, vol. 61, no. 1, pp. 252–256, Feb. 2014.

[19] G. Bizarri, W. W. Moses, J. Singh, A. N. Vasil'ev, and R. T. Williams, "An analytical model of nonproportional scintillator light yield in terms of recombination rates," *J. Appl. Phys.*, vol. 105, no. 4, Feb. 2009, Art. no. 044507.

[20] S. A. Payne, S. Hunter, L. Ahle, N. J. Cherepy, and E. Swanberg, "Nonproportionality of scintillator detectors. III. temperature dependence studies," *IEEE Trans. Nucl. Sci.*, vol. 61, no. 5, pp. 2771–2777, Oct. 2014.

[21] S. A. Payne, "Nonproportionality of scintillator detectors. IV. resolution contribution from delta-rays," *IEEE Trans. Nucl. Sci.*, vol. 62, no. 1, pp. 372–380, Feb. 2015.

[22] P. R. Beck, S. A. Payne, S. Hunter, L. Ahle, N. J. Cherepy, and E. L. Swanberg, "Nonproportionality of scintillator detectors. V. comparing the gamma and electron response," *IEEE Trans. Nucl. Sci.*, vol. 62, no. 3, pp. 1429–1436, Jun. 2015.

[23] W. W. Moses *et al.*, "The origins of scintillator non-proportionality," *IEEE Trans. Nucl. Sci.*, vol. 59, no. 5, pp. 2038–2044, Oct. 2012.

[24] H. Huang, Q. Li, X. Lu, Y. Qian, Y. Wu, and R. T. Williams, "Role of hot electron transport in scintillators: A theoretical study," *Phys. Status Solidi (RRL)-Rapid Res. Lett.*, vol. 10, no. 10, pp. 762–768, Sep. 2016.

[25] Q. Li, X. Lu, and R. T. Williams, "Toward a user's toolkit for modeling scintillator non-proportionality and light yield," *Proc. SPIE*, vol. 9213, Sep. 2014, Art. no. 92130K.

[26] M. Prange, D. Wu, Y. Xie, L. W. Campbell, F. Gao, and S. Kerisit, "Radiation response of inorganic scintillators: Insights from Monte Carlo simulations," *Proc. SPIE*, vol. 9213, Sep. 2014, Art. no. 92130L.

[27] M. P. Prange, Y. Xie, L. W. Campbell, F. Gao, and S. Kerisit, "Monte Carlo simulation of electron thermalization in scintillator materials: Implications for scintillator nonproportionality," *J. Appl. Phys.*, vol. 122, no. 23, Dec. 2017, Art. no. 234504.

[28] I. V. Khodyuk, J. T. M. de Haas, and P. Dorenbos, "Nonproportional response between 0.1–100 keV energy by means of highly monochromatic synchrotron X-rays," *IEEE Trans. Nucl. Sci.*, vol. 57, no. 3, pp. 1175–1181, Jun. 2010.

[29] M. Moszynski *et al.*, "Energy resolution and slow components in undoped CsI crystals," *IEEE Trans. Nucl. Sci.*, vol. 63, no. 2, pp. 459–466, Apr. 2016.

[30] S. Gridin *et al.*, "Pulse shape analysis of individual gamma events—Correlation to energy resolution and the possibility of its improvement," *J. Appl. Phys.*, vol. 124, no. 15, 2018, Art. no. 154504.

[31] A. Gektin and A. Vasil'ev, "Fluctuations of track structure and energy resolution of scintillators," in *Engineering of Scintillation Materials and Radiation Technologies* (Springer Proceedings in Physics), vol. 227, M. Korzhik and A. Gektin, Eds. Cham, Switzerland: Springer, 2019, pp. 29–39.

[32] A. N. Vasil'ev, "Microtheory of scintillation in crystalline materials," in *Engineering of Scintillation Materials and Radiation Technologies* (Springer Proceedings in Physics), vol. 200, A. Gektin and M. Korzhik, Eds. Cham, Switzerland: Springer, 2017, pp. 3–34.

[33] A. V. Gektin and A. N. Vasil'ev, "Fluctuations of ionizing particle track structure and energy resolution of scintillators," *Funct. Mater.*, vol. 24, no. 4, pp. 621–627, Dec. 2017.

[34] F. D. Brooks, "A scintillation counter with neutron and gamma-ray discriminators," *Nucl. Instrum. Methods*, vol. 4, no. 3, pp. 151–163, Apr. 1959.

[35] N. Zaitseva *et al.*, "Pulse shape discrimination in impure and mixed single-crystal organic scintillators," *IEEE Trans. Nucl. Sci.*, vol. 58, no. 6, pp. 3411–3420, Dec. 2011.

[36] A. Gektin and A. Vasil'ev, "Scintillator energy resolution and a way to improve it by kinetic waveform analysis," *Radiat. Meas.*, vol. 122, pp. 108–114, Mar. 2019.

[37] W. Wolszczak and P. Dorenbos, "Shape of intrinsic alpha pulse height spectra in lanthanide halide scintillators," *Nucl. Instrum. Methods Phys. Res. A, Accel., Spectrometers, Detectors Associated Equip.*, vol. 857, pp. 66–74, Jun. 2017.

[38] W. Wolszczak and P. Dorenbos, "Time-resolved gamma spectroscopy of single events," *Nucl. Instrum. Methods Phys. Res. A, Accel., Spectrometers, Detectors Associated Equip.*, vol. 886, pp. 30–35, Apr. 2018.

[39] A. V. Gektin, V. S. Suzdal, A. Yu Boyarintsev, and A. V. Sobolev, "Advanced method of scintillator energy resolution test," *Funct. Mater.*, vol. 26, no. 1, pp. 127–130, Mar. 2019.

[40] D. E. Cullen, J. H. Hubbell, and L. Kissel, "EPDL97: The evaluated photo data library97 version," Lawrence Livermore Nat. Lab., Livermore, CA, USA, Tech. Rep. UCRL-50400, 1997, vol. 6, no. 5.

[41] R. Kirkin, V. V. Mikhailin, and A. N. Vasil'ev, "Recombination of correlated electron–hole pairs with account of hot capture with emission of optical phonons," *IEEE Trans. Nucl. Sci.*, vol. 59, no. 5, pp. 2057–2064, Oct. 2012.

[42] G. Bizarri, W. W. Moses, J. Singh, A. N. Vasil'ev, and R. T. Williams, "The role of different linear and non-linear channels of relaxation in scintillator non-proportionality," *J. Lumin.*, vol. 129, no. 12, pp. 1790–1793, Dec. 2009.

[43] S. Gridin, A. Belsky, C. Dujardin, A. Gektin, N. Shiran, and A. Vasil'ev, "Kinetic model of energy relaxation in CsI:A (A = Tl and In) scintillators," *J. Phys. Chem. C*, vol. 119, no. 35, pp. 20578–20590, 2015.

[44] S. Gridin, A. N. Vasil'ev, A. Belsky, N. Shiran, and A. Gektin, "Excitonic and activator recombination channels in binary halide scintillation crystals," *Phys. Status Solidi (B)*, vol. 251, no. 5, pp. 942–949, Jan. 2014.

[45] S. Gridin *et al.*, "Carrier trap parameters in NaI with tl, in, and eu dopants," *J. Phys. Chem. C*, vol. 123, no. 22, pp. 13519–13530, May 2019.

[46] F. Gao, Y. Xie, S. Kerisit, L. W. Campbell, and W. J. Weber, "Yield, variance and spatial distribution of electron–hole pairs in CsI," *Nucl. Instrum. Methods Phys. Res. A, Accel., Spectrometers, Detectors Associated Equip.*, vol. 652, no. 1, pp. 564–567, 2011.

[47] J. MacQueen, "Some methods for classification and analysis of multivariate observations," in *Proc. 5th Berkeley Symp. Math., Stat. Probab.*, vol. 1, 1967, pp. 281–296.

[48] L. Kaufman, "Finding groups in data: An introduction to cluster analysis," in *Finding Groups in Data: An Introduction to Cluster Analysis*. New York, NY, USA: Wiley, 1990.

[49] R. O. Duda, P. E. Hart, and D. G. Stork, *Pattern Classification*. New York, NY, USA: Wiley, 2001.

[50] M. Kantardzic, *Data Mining: Concepts, Models, Methods, and Algorithms*. Hoboken, NJ, USA: Wiley, 2003.

[51] J. Han, M. Kamber, and J. Pei, *Data Mining: Concepts and Techniques*, 3rd ed. San Mateo, CA, USA: Morgan Kaufmann, 2011.

[52] I. H. Witten, E. Frank, and M. A. Hall, *Data Mining: Practical Machine Learning Tools and Techniques*, 3rd ed. Amsterdam, The Netherlands: Elsevier, 2011.

[53] R. Layton, *Learning Data Mining with Python*, 2nd ed. Birmingham U.K.: Packt, 2015.

[54] A. Gektin, A. Vasil'ev, V. Suzdal, I. Tawrovsky, and A. Sobolev, "Advanced approach to scintillator energy resolution," *Funct. Mater.*, vol. 27, no. 1, pp. 179–183, 2020.